Supereruptions in Northwestern Arabia Terra reveal an early stage of Mars's mantle evolution

Augustus Bates[1], Sander Goossens[2], Juan Manuel Lorenzo[3], Lujendra Ojha[4], Don R Hood[1], Suniti Kumara Karunatillake[1], Shannon Kobs Nawotniak[5], and Tyler Paladino[5]

[1]Louisiana State University
[2]University of Maryland, Baltimore County
[3]Louisana State University
[4]Rutgers University
[5]Idaho State University

November 24, 2022

Abstract

Martian meteoritic petrology and regional chemistry of Hesperian-Amazonian volcanism support secularly decreasing degrees of partial melting and thickening crust underlain by simple mantle convection. However, the applicability of this interior evolution model and resurfacing trends to the Noachian remains unknown. Using regional gamma spectroscopy and geophysical analysis, we find that supereruptions characterized Noachian volcanism in NW Arabia with co-enriched K, Th, and Si. Geophysical analysis reveals elastic thickness values below 20 km, indicating a heat flux exceeding many Hesperian volcanoes. Collectively, our results support large ion lithophile loss from low degrees of partial melting of the Noachian mantle, signifying an early stage of interior evolution that contrasts with the Hesperian-Amazonian model. Regional chemistry further suggests climate-altering supereruptive exhalations of ˜10^9 kg S-phases.

Supereruptions in Northwestern Arabia Terra reveal an early stage of Mars's mantle evolution

Authors: Augustus Bates[1]*, S. Goossens[2], J. M. Lorenzo[1], L. Ojha[3], D. R. Hood[4], S. Karunatillake[1], S. Kobs Nawotniak[5], T. Paladino[5]

[1]Department of Geology and Geophysics, Louisiana State University, Baton Rouge, LA, USA

[2] NASA Goddard Space Flight Center

[3]Rutgers, The State University of New Jersey

[4]Baylor University

[5]Idaho State University

*Corresponding author. Email: abate15@lsu.edu

Key Points:

1. Bulk chemistry and geophysical modeling of NW Arabia collectively support resurfacing from volcanic supereruptions.
2. Supereruptions were enriched in large ion lithophiles from low degrees of melting in the Noachian, a previously unknown early stage of interior evolution.
3. Regional chemistry indicates climate-altering supereruptive exhalations of mobile elements like S.

Abstract

Martian meteoritic petrology and regional chemistry of Hesperian-Amazonian volcanism support secularly decreasing degrees of partial melting and thickening crust underlain by simple mantle convection. However, the applicability of this interior evolution model and resurfacing trends to the Noachian remains unknown. Using regional gamma spectroscopy and geophysical analysis, we find that supereruptions characterized Noachian volcanism in NW Arabia with co-enriched K, Th, and Si. Geophysical analysis reveals elastic thickness values below 20 km, indicating a heat flux exceeding many Hesperian volcanoes. Collectively, our results support large ion lithophile loss from low degrees of partial melting of the Noachian mantle, signifying an early stage of interior evolution that contrasts with the Hesperian-Amazonian model. Regional chemistry further suggests climate-altering supereruptive exhalations of ~10^9 kg S-phases.

Plain Language Summary

The chemical evolution of the martian mantle has long been hypothesized to follow a simple monotonic trend in incompatible elements between the mantle and crust. Since incompatible elements partition into the melt first, on a planet with decreasing partial melting as the crust thickens without recycling (i.e. Mars) the abundance of these elements within extruded rocks would increase with increasing time or volcanic activity. We find that this model oversimplifies the distinctness of the martian mantle during the Noachian. In this study, we show that a Noachian-aged region on Mars exhibits regional geochemical trends that are consistent with explosive igneous activity and that the abundances of incompatible elements (K, Th) within this region suggest low partial melting. We corroborate these findings with estimations of elastic thickness and heat flux in this region.

1 Introduction

Resurfacing from voluminous, explosive volcanic eruptions can provide compositional insight into mantle-depth geology on Earth (Annen et al., 2006; Reid, 2008). While their martian counterparts during the Noachian may likewise constrain the chemical evolution of the early mantle, they are mostly uncharacterized due to scarce chemical evidence of confirmed Noachian volcanoes (Balta & McSween, 2013; Baratoux et al., 2011). Nevertheless, Noachian supereruptions (eruptions that expel a volume of material exceeding 450 km^3 (Baines & Sparks, 2005)) have been hypothesized for Mars (Michalski & Bleacher, 2013) and their existence

inferred through observations of expansive friable deposits (Bandfield et al., 2013; Michalski & Bleacher, 2013). Prior works propose super-eruptive paterae in NW Arabia (Michalski & Bleacher, 2013), and mineralogical evidence of their associated eruptions in stratigraphy (Whelley et al., 2021). Notably, these (Kerber et al., 2012; Whelley et al., 2021) are within an igneous chemical province (Taylor et al., 2010) of unknown provenance.

The chemistry of any supereruptions would provide a unique perspective into the melt processes of the martian mantle during the Noachian, while advancing prior mantle evolution models that were based on Hesperian-Amazonian regional geochemistry and martian meteorites. Some (i.e., Balta & McSween, 2013; Baratoux et al., 2011), predict an increase in incompatible elements (K, Th) within volcanic deposits through time corresponding to decreasing fractional melting (i.e., degree of partial melting), consequently necessitating highest fractional melting within the martian interior during the Noachian. Contrasting models, primarily based on thermal modelling, suggest rapid cooling of the martian mantle through significant (> 50%) removal of incompatible elements in forming the primary Noachian crust (Grott et al., 2012; Ojha, Karimi, et al., 2019; Plesa et al., 2015), leading to a secular decrease in incompatibles within volcanic deposits. Here we investigate which of these models best explains the geochemistry and geophysical data we have analyzed over NW Arabia.

2 Data and Methods

We identify a volcanic supereruption context region (SCR), located within a larger region (that we call broad SCR; BSCR), collectively bound by the chemical province in NW Arabia (Fig. 1). Accordingly, we delineate SCR and BSCR as distinct entities without overlapping chemical map pixels (derived from the Mars Odyssey Gamma Ray Spectroscopy, GRS, spectra),

maintaining consistency in mapped geology while also maximizing spatial extent to maintain sufficient coverage (> 10 pixels) for chemical analyses (Boynton et al., 2007; Carnes et al., 2017; Tanaka et al., 2014) (Fig. 1). Such GRS-derived chemical data are ideal for investigating regional trends in the bulk regolith, due to decimeter scale sampling depths and coarse spatial resolution throughout much of the mid-to-low latitudes (about 60^{o} to -60^{o}), with each pixel covering roughly 450 km (Boynton et al., 2007; Hood et al., 2016). While supereruptions could have a dispersed global footprint, SCR and BSCR target the area that would bear the thickest, most weathering-resistant, and compositionally representative units derived from potential supereruptions (Whelley et al., 2021; C. J. N. Wilson, 2008) tied to four putative Noachian paterae (Michalski & Bleacher, 2013).

We emphasize regional K-Th and S-Cl concentration trends because these four elements can effectively discriminate among alternative geochemical processes, such as volcanic (Baratoux et al., 2011), subaqueous deposition and alteration (Ehlmann et al., 2011; Taylor et al., 2006), and dust accumulation (Ojha et al., 2018). For example, K and Th fractionation trends can reveal the extent of aqueous alteration of soil and bedrock (basalt) in a region (Sawyer et al., 2000; Taylor et al., 2006, 2010). K and Th are also indicative of volcanic origins because they correlate strongly in igneous rocks as large ion lithophiles (LIL), in part due to their incompatibility with cation sites in silicates (Taylor et al., 2006).

We also compare S and Cl trends, because they are present in volatile phases of terrestrial volcanic degassing and may function similarly on Mars (Diez et al., 2009; Gaillard & Scaillet, 2009; Keller et al., 2006; Ojha et al., 2018; Ojha, Karunatillake, et al., 2019). As key volatiles, they can serve as a proxy for eruptive explosivity, and offer insight into mantle pressure regimes (Baratoux et al., 2011; Burton et al., 2009; Gasnault et al., 2010; Hood et al., 2016; Ojha et al.,

2018; Ojha, Karunatillake, et al., 2019; Spilliaert et al., 2006; Taylor et al., 2010). Furthermore, S and Cl have been used to characterize a global dust source region for Mars, through their consistent molar ratio observed in situ and within heavily mantled locales (Berger et al., 2016; Kerber et al., 2011; Ojha et al., 2018).

We complement our geochemical analyses with geophysical results from gravity and topography to estimate load density and elastic thickness of the lithosphere within SCR. Elastic thickness is a key parameter, as it represents the thickness of the deformable lithosphere, a proxy for heat flow and how coupled the lithosphere is to the mantle. As such, elastic thickness can offer insight into the thermal environment of a region (Belleguic et al., 2005; Grott & Wieczorek, 2012; McGovern et al., 2004) and the density of the crustal load provides insight into its composition (Ojha & Lewis, 2018).

Our investigations of regional geochemistry involve comparative analysis between SCR and other geologically unique regions on Mars. However, instead of an exhaustive set of regional chemical references, we consider specific regions which are geographically distributed for chemical comparisons (Fig. 1). This is because the early geologic history of Mars is difficult to interpret due to diverse chemical overprinting resulting from a multitude of processes, including magmatism (Balta & McSween, 2013; Baratoux et al., 2011, 2013), dust transport (Ojha et al., 2018) and aqueous alteration (Bibring et al., 2006; Ehlmann et al., 2011). Our comparative region selections maximize insight from diverse subaerial sedimentary and igneous processes and minimize bias from chemical overprinting across proximal regions (Table 1). We delineate these regions following topography and mapped geology (Tanaka et al., 2014) and compare subsequently using GRS-derived geochemistry.

3 Results and Discussion

The K and Th trends (Fig. 2A) within SCR are most consistent with igneous geochemistry of an enriched mantle source (Hefferan & O'Brien, 2010). SCR has the highest mean value of K and Th compared to the reference regions, a much lower dispersion in overall K and Th abundances in comparison to similarly enriched regions (i.e. Isidis and Apollinaris Mons), and a K/Th ratio resembling the crustal average (Table 1). A supereruption within SCR would have rapidly exhausted the source magma and terminated melting over a relatively short timescale (Scott et al., 2001). SCR's limited dispersion in K and Th (Fig. 2A) is consistent with fast and voluminous igneous emplacement. In contrast, the large dispersion in Th and lower abundances of K and Th observed for Apollinaris correspond to its ~2 Ma eruptive life (Robbins et al., 2011) that may span a chemical transition in the martian mantle (Balta & McSween, 2013).

The fast and voluminous emplacement indicated by the K and Th trends within SCR is unique among other regions on Mars. For example, our volcanic reference regions all appear to exhibit Th abundances consistent with mantle evolution models that suggest increasing abundances of incompatible elements with increasingly younger instances of magmatism (Fig. 2A, Table 1) (Balta & McSween, 2013; Baratoux et al., 2011). These volcanoes also have K/Th mass ratios that resemble the crustal average more than sedimentary references, though some variability in overall abundances of K and Th among the volcanic references is also evident. K and Th abundances are affected by the hydration state of the mantle (Balta & McSween, 2013), by variations in chemistry and melt processes of martian mantle sources driven in part by enriched pockets of residual melt near the crust mantle boundary (Basu Sarbadhikari et al., 2017), or by differing melt conditions (Baratoux et al., 2011; Hefferan & O'Brien, 2010). While these mechanisms may result in K/Th ratios that are distinct from the global spatial correlation,

K and Th abundances that strongly diverge from global linearity are generally due to secondary alteration (Taylor et al., 2006). This phenomenon is especially noticeable in our sedimentary reference regions (Fig. 2A), which consistently show a weaker bivariate correlation between K and Th, possibly from chemical weathering of igneous material that initially constituted the basin floors (Ehlmann et al., 2011; Taylor et al., 2006; Zalewska, 2013). In addition, our sedimentary references have K/Th ratios significantly above the crustal average (Table 1), consistent with low-pH alteration (Taylor et al., 2006; Zalewska, 2013).

Martian dust is enriched in S and Cl (Berger et al., 2016) and has been shown to exhibit a consistent molar ratio of S/Cl (Ojha et al., 2018), distinct from volcanic degassing (Gaillard & Scaillet, 2009; King & McLennan, 2010; Ojha et al., 2018; Ojha, Karunatillake, et al., 2019). Our calculated mean molar S/Cl ratio for SCR (~4.6) does not fall within the global dust molar ratio range (3.0 – 4.4) (Table 1; (Ehlmann et al., 2011; Kerber et al., 2011). The observed S enrichment in SCR (Fig. 2B), coupled with a S/Cl molar ratio diverging from that of martian dust (Ojha et al., 2018), supports sulfur adsorbed or chemically bound in the soil and regolith from volcanic degassing (Bibring et al., 2006; Ojha, Karunatillake, et al., 2019). Si and K abundances can provide additional corroboration, as dust mantled areas are generally depleted in these elements relative to the average crust (Berger et al., 2016; Lasue et al., 2018; Viviano et al., 2019). SCR is enriched in both Si and K (SI Appendix, Fig. S2) compared to the crust, further discounting compositional contributions from dust mantling within SCR.

Localized chemical weathering of basalt is unlikely to substantially enrich S and Cl (Diez et al., 2009). This is best exhibited in our Eridania reference, composed primarily of weathered volcanic material (Tanaka et al., 2014), exhibiting one of the lowest overall abundances of S and Cl reported in this study (Fig. 2B). Conversely, the Medusae Fossae Formation (MFF) has the

highest observed S and Cl values in this study (Fig. 2B), associated with its origin as a pyroclastic deposit from massive eruptions (Diez et al., 2009; Ojha & Lewis, 2018). This makes the MFF's S and Cl abundances key references for extensive explosive eruptions enhancing the volatile content of a region (Diez et al., 2009; Ojha et al., 2018). SCR is second in overall S and Cl abundances to Apollinaris (and by extension the MFF), which offers further support of volcanic degassing being the primary mechanism to enhance S and Cl within SCR (Diez et al., 2009; Ojha et al., 2018). Nevertheless, the distinctness in S/Cl ratios between SCR and MFF suggest that the pyroclastic deposits that may constitute SCR's chemistry do not serve as a major source of martian dust.

The observed S trends within SCR are consistent with K and Th trends, indicating that SCR's chemistry is not the result of aqueous alteration, despite a considerable enrichment in H_2O (SI Appendix, Fig. S2). If SCR hosted abundant fluvial activity, as its H_2O abundance may superficially suggest, S-phases would have been mobilized through interaction with water, resulting in substantial acidic weathering during the Middle to Late Noachian. Such sulfate-driven alteration is typically associated with ancient ground water systems on Mars (Zalewska, 2013), which would fractionate Th from K at low pH (Sawyer et al., 2000; Taylor et al., 2006). This would enrich the residual minerals in K, resulting in a K/Th ratio higher than that of the crust (Taylor et al., 2006), which is not observed at SCR (Table 1). In contrast, a high K/Th ratio is observed for Hellas, consistent with regional aqueous alteration within the basin (Zalewska, 2013). SCR shows little chemical similarity to Hellas within the scope of this study (Figs. 2 and 3), suggesting that SCR's observed S abundances are unrelated to sulfate deposits in aqueous (e.g., fluvial, playa, lacustrine) settings. There are many mechanisms which could have influenced SCR's H_2O abundance, such as pyroclastic scavenging of atmospheric vapor, which

188 is primarily dictated by particle fall time through the atmosphere (Wilson & Head, 2007).
189 Consequently, the simultaneous enrichment of H_2O along with S and Cl, given the rest of the
190 chemical context of SCR, is more consistent with a highly explosive volcanic provenance.

191 Geophysical modeling also supports the geochemical evidence for SCR's supereruptive
192 provenance. We use admittance analysis from gravity and topographic data to provide estimates
193 of the elastic thickness of the lithosphere and a range of potential densities for the loads (see SI
194 for details). We use elastic thickness estimates as proxies for regional thermal flux (Belleguic et
195 al., 2005; McGovern et al., 2004), which has implications for SCR's inferred eruptive regime.
196 SCR's low elastic thickness of ~15 km (Fig. 3) roughly corresponds to a thermal gradient
197 exceeding 19 K/km and a heat flux between 47 and 75 mW/m^2, a range higher than for some
198 martian volcanoes (Karimi et al., 2016; McGovern et al., 2004). This estimate resembles prior
199 heat flow estimates (Belleguic et al., 2005; McGovern et al., 2004) which report similar elastic
200 thickness values within the Arabia region. The increased thermal flux associated with
201 predominantly low elastic thickness values for SCR is in turn consistent with both a mantle
202 plume beneath SCR and enrichment of radioactive elements like K and Th (Michael, 1995).

203 Our geophysical analyses also yield a load density for SCR resembling the low densities
204 for MFF (Ojha & Lewis, 2018), consistent with thick pyroclastic deposits. The regional load
205 density as obtained from gravity and topography (Fig. 3; SI Appendix, Fig. S3) is on average
206 lower than 1900 kg/m^3. Deposition of friable material derived from supereruptions with
207 associated low top load density can arise from more buoyant magma containing dissolved gases
208 (McSween Jr., 1994). Our estimated load density also constrains the amount of degassed sulfur
209 from eruptions. Using the erupted volume estimated for one patera within SCR by (Michalski &
210 Bleacher, 2013), and an average density of 1800 kg/m^3 (Fig. 3), we estimate a 12×10^9 kg

maximum mass of erupted material. Of this total mass, approximately 2.8×10^8 kg is sulfur, based on our measured S abundances within SCR (averaging 2.4 wt%; Table 1). If this mass represents the 30% which was scavenged by ash, a percentage consistent with conservative estimates of atmospheric degassing (Ojha, Karunatillake, et al., 2019), the remaining mass of sulfur degassed to the atmosphere is approximately 6.5×10^8 kg. Considering all four paterae with volumetrically similar concurrent eruptions, the amount of degassed sulfur increases to 2.6×10^9 kg. For comparison, the Toba eruption, the largest Quaternary volcanic eruption on Earth, emitted 10^{10}-10^{12} kg of sulfur (c.f. Ojha et al., 2018). If eruptions within SCR were brief and clustered temporally, such amounts of degassed sulfur alone would have impacted global climate (Halevy et al., 2007; Rampino & Self, 1992; Tian et al., 2010).

Given the evidence for volcanogenic Cl and S within SCR, the mantle context of the eruptions can also be considered. The average elemental abundances of S and Cl within SCR (≥ 3wt%; Table 1) suggest that the magma source had a relatively high abundance of dissolved volatiles, which would lead to explosive eruptions that rival terrestrial supereruptions (Hefferan & O'Brien, 2010; Spilliaert et al., 2006). Shallow melting of even a dry mantle source can produce S-enriched magma, as S exsolves into the vapor phase at low pressures within drier magmas, also increasing the potential for explosive eruptions (Burton et al., 2009; Spilliaert et al., 2006). In addition, we observe an enrichment in Ca (SI Appendix, Fig. S2), consistent with more Ca-rich pyroxenes within the primary melt at this time relative to succeeding eons (Baratoux et al., 2013). We also observe a Si enrichment (SI Appendix, Fig. S2) within SCR which would cause the high melt viscosities implied for older, more explosive volcanism (Baratoux et al., 2011). SCR additionally exhibits similar degrees of enrichment in K and Cl

compared to the martian crust (SI Appendix, Fig. S2), consistent with their typical correlation within terrestrial basalts (Workman et al., 2006).

Based on a Middle Noachian age for SCR, any eruptions were likely sourced from a hotter mantle with less confining pressure (Baratoux et al., 2011). This would suggest that any eruptions would have high degrees of partial melting (Baratoux et al., 2011), which contrasts with the observed abundances of K and Th (Fig. 2). However, large ion lithophile abundance may not be as representative of the chemical evolution of the martian mantle through time as posited by some mantle evolution models (i.e, Balta & McSween, 2013; Baratoux et al., 2011). Younger and older volcanoes differ categorically in Si abundance, but Th and Fe abundances overlap among age groups (Baratoux et al., 2011; Hahn, B C, Mclennan, 2007). Since Th abundance is inversely related to the amount of partial melting prior to eruption, the overlap in Th abundance among older and younger volcanoes reveals that partial melting may not follow a monotonic temporal trend. This contradicts the predictions of key petrologically-based mantle evolution models (i.e., Balta & McSween, 2013; Baratoux et al., 2011) from regional and meteoritic geochemistry.

The observed compositional trends provide additional insight on an evolving mantle composition. If eruptive chemistry primarily represents sampling of a heterogeneous martian crust, consistent trends in Si and Th with age become less likely, as Hesperian to Amazonian volcanic provinces are not collocated, and therefore must be sampling the crust at different depths and in different ways (Annen et al., 2006). Indeed, on Earth, the intermingling of residual melt and crustal melt is responsible for much of the observed heterogeneity among surface expressions of magmatism (Annen et al., 2006). However, on Mars, crustal compositional heterogeneity is subdued compared to Earth (Baratoux et al., 2014), and the mantle is considered

generally less dynamic (Ruiz et al., 2011), suggesting that eruptive chemical changes are primarily driven by changing mantle composition (Balta & McSween, 2013). Thus, the temporally consistent trend in Si likely reflects a changing mantle composition wherein magmas experience similar degrees of compositional dilution from crustal assimilation, likely due to a substantially thick crust, among post-Noachian, martian volcanoes. Our study shows that SCR has the thermal properties of Noachian volcanoes (Fig. 3) (Baratoux et al., 2011; McGovern et al., 2004), but with a surface chemistry that is unique (Fig. 2). This chemistry indicates a compositionally distinct mantle source among contemporaneous volcanoes, capable of producing explosive eruptions.

4 Conclusions

From our collective observations, we hypothesize that a massive, volatile-enriched, mantle plume underwent low fractional melting (Workman et al., 2006) in the Noachian to yield a regional magma body, enriched in LILs like K and Th. Low fractional melting is imperative to cause SCR's Th enrichment, unlike the sometimes lower Th across older volcanic provinces compared to younger counterparts (Balta & McSween, 2013; Baratoux et al., 2011). The deviation from the temporal trend in Th used in prior mantle evolution models would be consistent with SCR's distinctness compared to other volcanic provinces, as reflected in supereruptions (Gravley et al., 2016; Reid, 2008; Taylor et al., 2010). The possibility of explosive eruptions from Si and volatile (S, Cl) enriched Noachian melts is broadly consistent with geomorphic and thermophysical evidence of explosive volcanic resurfacing in the Noachian (Bandfield et al., 2013). Low confining pressure from a thermally eroded local lithosphere – as consistent with our geophysical analyses – may have further enhanced explosivity.

The temporally and spatially localized explosive eruptions we infer early in martian history are consistent with massive, climate-transforming, volatile injections into the atmosphere (Ojha, Karunatillake, et al., 2019). If such eruptions were pervasive during the Noachian, it would dramatically affect the stability and availability of water on the martian surface (Halevy et al., 2007; Tian et al., 2010). The possible onset of glaciation from the explosive eruptions and sulfur degassing (Halevy et al., 2007; Tian et al., 2010) within SCR would affect surface habitability, likely driving those habitable zones underground where it was warmer. Furthermore, the regional magma body that fed eruptions within SCR likely remained thermally active long after the termination of surface volcanism (Annen & Sparks, 2002). Deep crustal intrusion zones, such as the one we hypothesize for SCR, can take millions of years to return to the global geothermal gradient state (Annen & Sparks, 2002). Future investigations of the larger chemical province that houses SCR focused on regolith mixing processes would help deconvolve varying compositional input from the diverse geologic units in the area. The contrast in SCR's chemistry with key models of martian mantle evolution (Balta & McSween, 2013; Baratoux et al., 2011), also reinforces regional heterogeneity in mantle processes and makes NW Arabia an ideal endmember to refine the models.

Acknowledgments: Dr. Joe Levy provided topical advice on the manuscript.

Funding: AB was funded by NASA-Mars Data Analysis Program grant 80NSSC18K1375 to SK, Louisiana NASA EPSCoR under cooperative agreement 80NSSC20M0150 (CFDA #43.008) to JML, and teaching assistantship in Geology & Geophysics at LSU. DRH, TP and SKN were also supported by 80NSSC18K1375.

Author contributions: AB, SK, SG designed research; AB, SG performed research; SK (deriving chemistry from gamma spectra) and JML (geophysics) guided the data analysis and interpretations also as the dissertation advisors; DRH contributed to reference region selection, LO to geophysical interpretations, TP and SKN on volcanic eruptions. AB, SG analyzed data; AB wrote the manuscript with participation by all co-authors.

Competing interests: Authors declare that they have no competing interests.

Data and materials availability: Mapped geology for Mars was acquired from the USGS archive (https://pubs.usgs.gov/sim/3292/) developed by Tanaka et al., (2014) and subsequent analysis of this data was performed using ArcGIS software. GRS spectra are from the NASA Planetary Database System (PDS, https://pds-geosciences.wustl.edu/missions/odyssey/grs_cgs.html). Topographic data are from the Mars Orbiter Laser Altimeter (MOLA) data, also archived at NASA PDS, and used in the MarsTopo2600 model (Wieczorek, 2015, see https://figshare.com/articles/dataset/Spherical_harmonic_model_of_the_shape_of_Mars_MarsTopo2600/12402653). The gravity model used in our analysis can be found at the NASA/GSFC PGDA website (https://pgda.gsfc.nasa.gov/products/63). Details of data sources follow in their respective sections.

Supplementary Materials

Materials and Methods

Supplementary Text

Figs. S1 to S3

Table S1

References (*1-44*)

References

Annen, C., & Sparks, R. S. J. (2002). Effects of repetitive emplacement of basaltic intrusions on thermal evolution and melt generation in the crust. *Earth and Planetary Science Letters*, *203*(3–4), 937–955. https://doi.org/10.1016/S0012-821X(02)00929-9

Annen, C., Blundy, J. D., & Sparks, R. S. J. (2006). The genesis of intermediate and silicic magmas in deep crustal hot zones. *Journal of Petrology*, *47*(3), 505–539. https://doi.org/10.1093/petrology/egi084

Baines, P. G., & Sparks, R. S. J. (2005). Dynamics of giant volcanic ash clouds from supervolcanic eruptions. *Geophysical Research Letters*, *32*(24), 1–4. https://doi.org/10.1029/2005GL024597

Balta, J. B., & McSween, H. Y. (2013). Water and the composition of Martian magmas. *Geology*, *41*(July), 1115–1118. https://doi.org/10.1130/G34714.1

Bandfield, J. L., Edwards, C. S., Montgomery, D. R., & Brand, B. D. (2013). The dual nature of the martian crust: Young lavas and old clastic materials. *Icarus*, *222*(1), 188–199. https://doi.org/10.1016/j.icarus.2012.10.023

Baratoux, D., Toplis, M. J., Monnereau, M., & Gasnault, O. (2011). Thermal history of Mars inferred from orbital geochemistry of volcanic provinces. *Nature*, *472*(7343), 338–41. https://doi.org/10.1038/nature09903

Baratoux, D., Toplis, M. J., Monnereau, M., & Sautter, V. (2013). The petrological expression of early Mars volcanism. *Journal of Geophysical Research E: Planets*, *118*(1), 59–64. https://doi.org/10.1029/2012JE004234

Baratoux, D., Samuel, H., Michaut, C., Toplis, M. J., Monnereau, M., Wieczorek, M., et al. (2014). Petrological constraints on the density of the Martian crust. *Journal of Geophysical*

Research, *119*, 1707–1727. https://doi.org/10.1002/2014JE004642

Basu Sarbadhikari, A., Babu, E. V. S. S. K., & Vijaya Kumar, T. (2017). Chemical layering in the upper mantle of Mars: Evidence from olivine-hosted melt inclusions in Tissint. *Meteoritics and Planetary Science*, *52*(2), 251–267. https://doi.org/10.1111/maps.12790

Belleguic, V., Lognonné, P., & Wieczorek, M. (2005). Constraints on the Martian lithosphere from gravity and topography data. *Journal of Geophysical Research E: Planets*, *110*(11), 1–22. https://doi.org/10.1029/2005JE002437

Berger, J. A., Schmidt, M. E., Gellert, R., Campbell, J. L., King, P. L., Flemming, R. L., et al. (2016). A global Mars dust composition refined by the Alpha-Particle X-ray Spectrometer in Gale Crater. *Geophysical Research Letters*, *43*(1), 67–75. https://doi.org/10.1002/2015GL066675

Bibring, J.-P., Langevin, Y., Mustard, J. F., Poulet, F., Arvidson, R., Gendrin, A., et al. (2006). Global mineralogical and aqueous mars history derived from OMEGA/Mars Express data. *Science (New York, N.Y.)*, *312*(5772), 400–404. https://doi.org/10.1126/science.1122659

Boynton, W. V., Taylor, G. J., Evans, L. G., Reedy, R. C., Starr, R., Janes, D. M., et al. (2007). Concentration of H, Si, Cl, K, Fe, and Th in the low- and mid-latitude regions of Mars. *Journal of Geophysical Research*, *112*, E12S99. https://doi.org/10.1029/2007JE002887

Burton, M. R., Caltabiano, T., Murè, F., Salerno, G., & Randazzo, D. (2009). SO2 flux from Stromboli during the 2007 eruption: Results from the FLAME network and traverse measurements. *Journal of Volcanology and Geothermal Research*, *182*(3–4), 214–220. https://doi.org/10.1016/j.jvolgeores.2008.11.025

Carnes, L. L., Karunatillake, S., Susko, D. A., & Hood, D. R. (2017). Delineating the Arabia Terra region on Mars to investigate paterae orgins. In *LPSC2017* (p. Abstract 1756).

https://doi.org/10.1038/ngeo2845

Diez, B., Feldman, W. C., Mangold, N., Baratoux, D., Maurice, S., Gasnault, O., et al. (2009). Contribution of Mars Odyssey GRS at Central Elysium Planitia. *Icarus*, *200*(1), 19–29. https://doi.org/10.1016/j.icarus.2008.11.011

Ehlmann, B. L., Mustard, J. F., Murchie, S. L., Bibring, J.-P., Meunier, A., Fraeman, A. a, & Langevin, Y. (2011). Subsurface water and clay mineral formation during the early history of Mars. *Nature*, *479*(7371), 53–60. https://doi.org/10.1038/nature10582

Gaillard, F., & Scaillet, B. (2009). The sulfur content of volcanic gases on Mars. *Earth and Planetary Science Letters*, *279*(1–2), 34–43. https://doi.org/10.1016/j.epsl.2008.12.028

Gasnault, O., Jeffrey Taylor, G., Karunatillake, S., Dohm, J., Newsom, H., Forni, O., et al. (2010). Quantitative geochemical mapping of martian elemental provinces. *Icarus*, *207*(1), 226–247. https://doi.org/10.1016/j.icarus.2009.11.010

Gravley, D. M., Deering, C. D., Leonard, G. S., & Rowland, J. V. (2016). Ignimbrite flare-ups and their drivers: A New Zealand perspective. *Earth-Science Reviews*, *162*, 65–82. https://doi.org/10.1016/j.earscirev.2016.09.007

Grott, M., & Wieczorek, M. A. (2012). Density and lithospheric structure at Tyrrhena Patera, Mars, from gravity and topography data. *Icarus*, *221*(1), 43–52. https://doi.org/10.1016/j.icarus.2012.07.008

Grott, M., Baratoux, D., Hauber, E., Sautter, V., Mustard, J. F., Gasnault, O., et al. (2012). Long-Term Evolution of the Martian Crust-Mantle System. *Space Science Reviews*, *174*(1–4), 49–111. https://doi.org/10.1007/s11214-012-9948-3

Hahn, B C, Mclennan, S. M. (2007). Evolution and Geochemistry of the Martian Crust: Integrating Mission Datasets. In *Seventh International Conference on Mars*. Pasadena, CA:

399 Lunar and Planetary Institute. Retrieved from
400 https://www.lpi.usra.edu/meetings/7thmars2007/pdf/3179.pdf
401 Halevy, I., Zuber, M. T., & Schrag, D. P. (2007). A Sulfur Dioxide Climate Feedback on Early
402 Mars. *Science*, *318*(December), 1903–1908. https://doi.org/10.5040/9780755621101.0007
403 Hefferan, K., & O'Brien, J. (2010). Magma and Intrusive Structures. In *Earth Materials* (1st ed.,
404 pp. 212–227). John Wiley & Sons, Ltd.
405 Hood, D. R., Judice, T., Karunatillake, S., Rogers, D., Dohm, J. M., Susko, D. A., & Carnes, L.
406 K. (2016). Assessing the geologic evolution of Greater Thaumasia, Mars. *Journal of*
407 *Geophysical Research: Planets*, *121*(9), 1753–1769. https://doi.org/10.1002/2016JE005046
408 Karimi, S., Dombard, A. J., Buczkowski, D. L., Robbins, S. J., & Williams, R. M. (2016). Using
409 the viscoelastic relaxation of large impact craters to study the thermal history of Mars.
410 *Icarus*, *272*, 102–113. https://doi.org/10.1016/j.icarus.2016.02.037
411 Keller, J. M., Boynton, W. V., Karunatillake, S., Baker, V. R., Dohm, J. M., Evans, L. G., et al.
412 (2006). Equatorial and midlatitude distribution of chlorine measured by Mars Odyssey
413 GRS. *Journal of Geophysical Research*, *112*(E3), E03S08.
414 https://doi.org/10.1029/2006JE002679
415 Kerber, L., Head, J. W., Madeleine, J. B., Forget, F., & Wilson, L. (2011). The dispersal of
416 pyroclasts from Apollinaris Patera, Mars: Implications for the origin of the Medusae Fossae
417 Formation. *Icarus*, *216*(1), 212–220. https://doi.org/10.1016/j.icarus.2011.07.035
418 Kerber, L., Head, J. W., Madeleine, J.-B., Forget, F., & Wilson, L. (2012). The dispersal of
419 pyroclasts from ancient explosive volcanoes on Mars: Implications for the friable layered
420 deposits. *Icarus*, *219*(1), 358–381. https://doi.org/10.1016/j.icarus.2012.03.016
421 King, P. L., & McLennan, S. M. (2010). Sulfur on Mars. *Elements*, *6*(2), 107–112.

https://doi.org/10.2113/gselements.6.2.107

Lasue, J., Cousin, A., Meslin, P. Y., Mangold, N., Wiens, R. C., Berger, G., et al. (2018). Martian Eolian Dust Probed by ChemCam. *Geophysical Research Letters*, *45*(20), 10,968-10,977. https://doi.org/10.1029/2018GL079210

McGovern, P. J., Solomon, S. C., Smith, D. E., Zuber, M. T., Simons, M., Wieczorek, M. A., et al. (2004). Correction to "Localized gravity/topography admittance and correlation spectra on Mars: Implications for regional and global evolution." *Journal of Geophysical Research E: Planets*, *109*(12), 19–1. https://doi.org/10.1029/2002je001854

McSween Jr., H. Y. (1994). What we have learned about Mars from SNC meteorites. *Meteoritics*, *29*(1 994), 757–779. Retrieved from http://articles.adsabs.harvard.edu/full/thumbnails/seri/Metic/0029/1994Metic..29..757M.html

Michael, P. (1995). Regionally distinctive sources of depleted MORB: Evidence from trace elements and H2O. *Earth and Planetary Science Letters*, *131*(3–4), 301–320. https://doi.org/10.1016/0012-821X(95)00023-6

Michalski, J. R., & Bleacher, J. E. (2013). Supervolcanoes within an ancient volcanic province in Arabia Terra, Mars. *Nature*, *502*(7469), 47–52. https://doi.org/10.1038/nature12482

Ojha, L., & Lewis, K. (2018). The Density of the Medusae Fossae Formation: Implications for its Composition, Origin, and Importance in Martian History. *Journal of Geophysical Research: Planets*, *123*(6), 1368–1379. https://doi.org/10.1029/2018JE005565

Ojha, L., Lewis, K., Karunatillake, S., & Schmidt, M. (2018). The Medusae Fossae Formation as the single largest source of dust on Mars. *Nature Communications*, *9*(1), 1–7. https://doi.org/10.1038/s41467-018-05291-5

Ojha, L., Karunatillake, S., & Lacovino, K. (2019). Atmospheric Injection of Sulfur from the Medusae Fossae Forming Events. *Planetary and Space Science*, *179*, 104734. https://doi.org/10.1016/j.pss.2019.104734

Ojha, L., Karimi, S., Lewis, K. W., Smrekar, S. E., & Siegler, M. (2019). Depletion of Heat Producing Elements in the Martian Mantle. *Geophysical Research Letters*, *46*(22), 12756–12763. https://doi.org/10.1029/2019GL085234

Plesa, A. C., Tosi, N., Grott, M., & Breuer, D. (2015). Thermal evolution and Urey ratio of Mars. *Journal of Geophysical Research: Planets*, *120*(5), 995–1010. https://doi.org/10.1002/2014JE004748

Rampino, M. R., & Self, S. (1992). Volcanic Winter and Accelerated Glaciation Following the Toba Super-Eruption. *Nature*, *359*(September), 50–52.

Reid, M. R. (2008). How long does it take to supersize an eruption. *Elements*, *4*(1), 23–28. https://doi.org/10.2113/GSELEMENTS.4.1.23

Robbins, S. J., Di Achille, G., & Hynek, B. M. (2011). The volcanic history of Mars: High-resolution crater-based studies of the calderas of 20 volcanoes. *Icarus*, *211*(2), 1179–1203. https://doi.org/10.1016/j.icarus.2010.11.012

Ruiz, J., McGovern, P. J., Jiménez-Díaz, A., López, V., Williams, J.-P., Hahn, B. C., & Tejero, R. (2011). The thermal evolution of Mars as constrained by paleo-heat flows. *Icarus*, *215*(2), 508–517. https://doi.org/10.1016/j.icarus.2011.07.029

Sawyer, D. J., McGehee, M. D., Canepa, J., & Moore, C. B. (2000). Water soluble ions in the Nakhla martian meteorite. *Meteoritics and Planetary Science*, *35*(4), 743–747. https://doi.org/10.1111/j.1945-5100.2000.tb01458.x

Scott, E. D., Wilson, L., & Head, J. W. (2001). Evidence for episodicity in the magma supply to

the large Tharsis Volcanoes. *Journal Geophysical Research*, *106*, 1423–1433.

Spilliaert, N., Allard, P., Métrich, N., & Sobolev, A. V. (2006). Melt inclusion record of the conditions of ascent, degassing, and extrusion of volatile-rich alkali basalt during the powerful 2002 flank eruption of Mount Etna (Italy). *Journal of Geophysical Research: Solid Earth*, *111*(4). https://doi.org/10.1029/2005JB003934

Tanaka, K. L., Robbins, S. J., Fortezzo, C. M., Skinner, J. A., & Hare, T. M. (2014). The digital global geologic map of Mars: Chronostratigraphic ages, topographic and crater morphologic characteristics, and updated resurfacing history. *Planetary and Space Science*, *95*, 11–24. https://doi.org/10.1016/j.pss.2013.03.006

Taylor, G. J., Stopar, J. D., Boynton, W. V., Karunatillake, S., Keller, J. M., Brückner, J., et al. (2006). Variations in K/Th on Mars. *Journal of Geophysical Research*, *112*(E3), E03S06. https://doi.org/10.1029/2006JE002676

Taylor, G. J., Martel, L. M. V., Karunatillake, S., Gasnault, O., & Boynton, W. V. (2010). Mapping Mars geochemically. *Geology*, *38*(2), 183–186. https://doi.org/10.1130/G30470.1

Tian, F., Claire, M. W., Haqq-Misra, J. D., Smith, M., Crisp, D. C., Catling, D., et al. (2010). Photochemical and climate consequences of sulfur outgassing on early Mars. *Earth and Planetary Science Letters*, *295*(3–4), 412–418. https://doi.org/10.1016/j.epsl.2010.04.016

Viviano, C., Murchie, S. L., Daubar, I. J., Morgan, M. F., Seelos, F. P., & Plescia, J. B. (2019). Composition of Amazonian volcanic materials in Tharsis and Elysium, Mars, from MRO/CRISM reflectance spectra. *Icarus*, #pagerange#. https://doi.org/10.1016/j.icarus.2019.03.001

Whelley, P., Matiella Novak, A., Richardson, J., Bleacher, J., Mach, K., & Smith, R. N. (2021). Stratigraphic Evidence for Early Martian Explosive Volcanism in Arabia Terra.

Geophysical Research Letters, *48*(15), 1–12. https://doi.org/10.1029/2021gl094109

Wieczorek, M. A. (2008). Constraints on the composition of the martian south polar cap from gravity and topography. *Icarus*, *196*(2), 506–517. https://doi.org/10.1016/j.icarus.2007.10.026

Wilson, C. J. N. (2008). Supereruptions and supervolcanoes: Processes and products. *Elements*, *4*(1), 29–34. https://doi.org/10.2113/GSELEMENTS.4.1.29

Wilson, L., & Head, J. W. (2007). Explosive volcanic eruptions on Mars: Tephra and accretionary lapilli formation, dispersal and recognition in the geologic record. *Journal of Volcanology and Geothermal Research*, *163*(1–4), 83–97. https://doi.org/10.1016/j.jvolgeores.2007.03.007

Workman, R. K., Hauri, E., Hart, S. R., Wang, J., & Blusztajn, J. (2006). Volatile and trace elements in basaltic glasses from Samoa: Implications for water distribution in the mantle. *Earth and Planetary Science Letters*, *241*(3–4), 932–951. https://doi.org/10.1016/j.epsl.2005.10.028

Zalewska, N. (2013). Hellas Planitia as a potential site of sedimentary minerals. *Planetary and Space Science*, *78*, 25–32. https://doi.org/10.1016/j.pss.2012.12.006

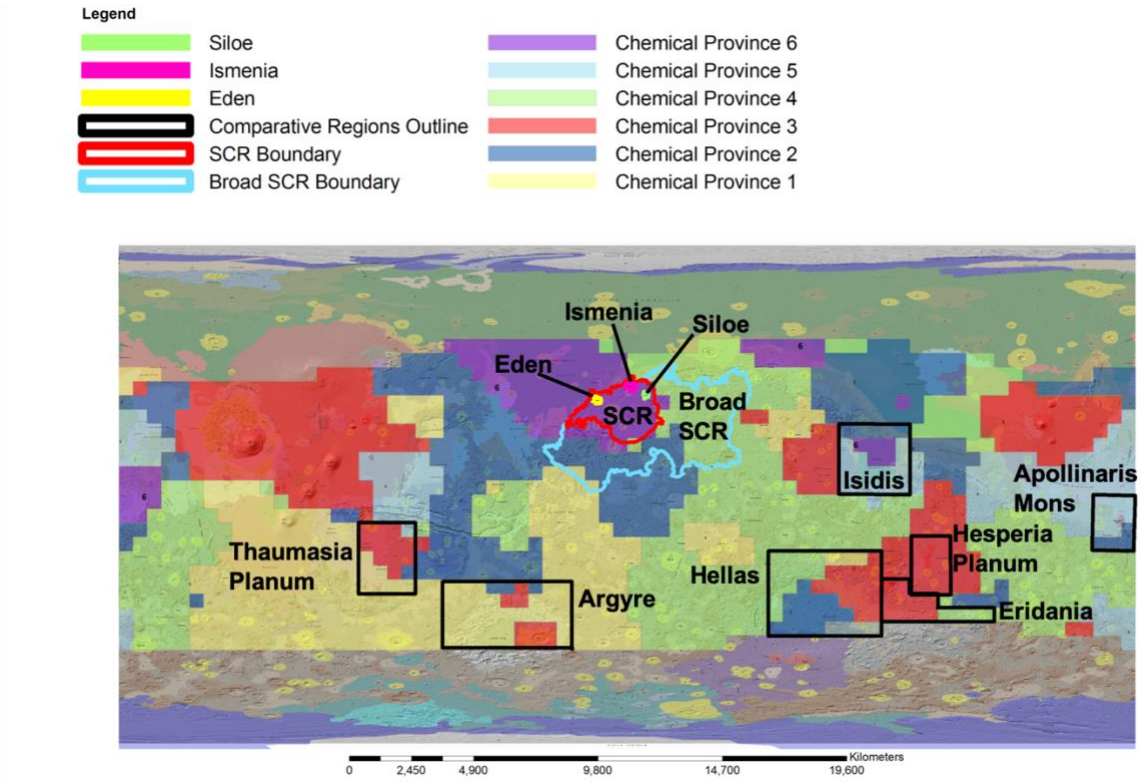

Fig. 1: Geologic map of Mars (Tanaka et al., 2014) with Taylor et al.'s geochemical provinces (Taylor et al., 2010) overlain. SCR and BSCR derived by us are shown along with three previously proposed paterae (Siloe, Ismenia, and Eden) by (Michalski & Bleacher, 2013). We delineated SCR using a combination of mapped geology, regional chemistry and topography, to ensure that geologic and chemical consistency within SCR was maintained. Thus, SCR is composed entirely of chemical Province 6 by (Taylor et al., 2010). BSCR represents the more heterogeneous Arabia region that surrounds SCR, which was also delineated using mapped geology, chemistry and topography. The black boxes outline comparative regions for compositional study. Our basin references are Argyre, Hellas and Isidis. Our volcanic references are Thaumasia and Hesperia Planae and Apollinaris Mons. We also selected a region to the east of Hellas (Eridania) which is composed of heavily eroded fluvial and volcanic material. More details on region selection can be found in section 1 of the Appendix.

Table 1: Average chemistry for each martian reference region, spatial extent in chemical map pixels, and geologic analog context for which they served as a reference. Underlying chemical data are the same as used in Figures 1 and 2. Values for SCR, BSCR and the martian crust are also given. The crustal proxy has SCR and BSCR removed to reduce sampling bias. Overall, our reference regions are close temporal counterparts to SCR. The mean mass fraction for K, Th, S and Cl is given for all the regions with K and Th reported in mg/kg and S and Cl reported as percentages (wt%). The ratios for K/Th and S/Cl are calculated from reported elemental weight percent. The 1 sigma error is the standard error of the mean; ratio error is calculated by $(K/Th)[(\sigma_K/K)^2+(\sigma_{Th}/Th)^2]^{1/2}$, where K and Th are the mean concentration of K, Th. The same applies to S and Cl.

Region Name	Geologic Analog	Age (Ga)	Average Elemental Abundance (K & Th in mg/kg, S & Cl in wt%) (1σ error)	
Hellas (48 Pixels)	Impact formed, Sedimentary Basin	~ 4.1	K: 3007 ± 145.2	S: 2.1 ± 0.3
			Th: 0.41 ± 0.06	Cl: 0.4 ± 0.04
			K/Th: 7325 ± 1138	S/Cl: 5.1 ± 0.8
Argyre (41 Pixels)	Impact formed, Sedimentary Basin	~ 4.0	K: 3021.6 ± 107.8	S: 1.9 ± 0.2
			Th: 0.49 ± 0.04	Cl: 0.38 ± 0.03
			K/Th: 6144.9 ± 601	S/Cl: 5.0 ± 0.7
Isidis (25 Pixels)	Impact Induced Magmatism	~ 3.9 – 3.8	K: 3860.4 ± 120.6	S: 1.9 ± 0.2
			Th: 0.69 ± 0.05	Cl: 0.49 ± .03
			K/Th: 5625 ± 477	S/Cl: 3.9 ± 0.5
Eridania (14 Pixels)	Heavily Weathered Fine-Grained Material (multiple sources)	~ 4.0 – 3.7	K: 3099 ± 92.4	S: 1.9 ± 0.3
			Th: 0.5 ± 0.04	Cl: 0.38 ± 0.03
			K/Th: 6190.2 ± 573	S/Cl: 5.1 ± 0.8
Thaumasia Planum (20 Pixels)	Volcanic Site	~ 3.8 – 3.7	K: 2657 ± 67.3	S: 2.0 ± 0.2
			Th: 0.4 ± .03	Cl: 0.41 ± 0.03
			K/Th: 6581.5 ± 588	S/Cl: 4.9 ± 0.6
Hesperia Planum (12 Pixels)	Volcanic Site	~ 3.7	K: 2655.5 ± 81.5	S: 2.0 ± 0.2
			Th: 0.44 ± 0.04	Cl: 0.43 ± 0.03
			K/Th: 6035.2 ± 581	S/Cl: 4.7 ± 0.6
Apollinaris Mons (12 Pixels)	Volcanic Site	~ 3.6 – 3.8	K: 3331 ± 104	S: 2.6 ± 0.2
			Th: 0.63 ± 0.05	Cl: 0.66 ± 0.04
			K/Th: 5325 ± 451	S/Cl: 3.9 ± 0.4
SCR (Arabia) (23 Pixels)	Proposed Volcanic Site	~ 3.9 – 3.8	K: 3990.8 ± 117.6	S: 2.4 ± 0.3
			Th: 0.74 ± 0.05	Cl: 0.52 ± 0.04
			K/Th: 5372 ± 419	S/Cl: 4.6 ± 0.6
Broad SCR (Arabia) (48 Pixels)	Larger Region Housing SCR	~ 3.9 – 3.8	K: 3684 ± 118.7	S: 2.3 ± 0.2
			Th: 0.69 ± 0.06	Cl: 0.49 ± 0.03
			K/Th: 5336.7 ± 460	S/Cl: 4.7 ± 0.6
Martian Crustal Proxy (1358 Pixels)	(Excluding SCR and Broad SCR)		K: 3523 ± 100.7	S: 2.2 ± 0.23
			Th: 0.61 ± 0.05	Cl: 0.46 ± 0.03
			K/Th: 5783.7 ± 474	S/Cl: 4.8 ± 0.6

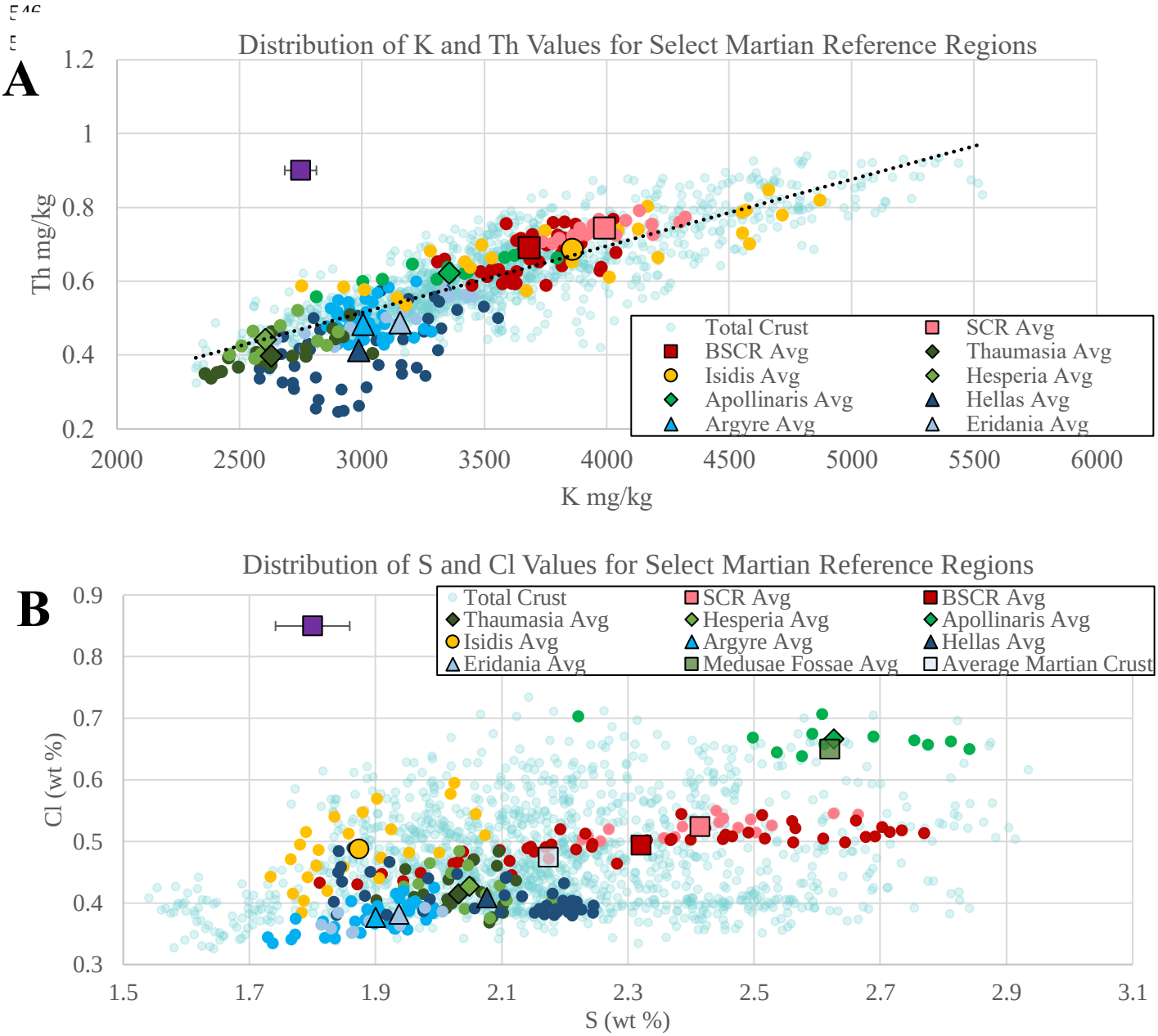

Fig. 2: (A) Mean K and Th values (large polygons), along with the underlying data (small circles) used to calculate the mean for reference regions on Mars - and the mid to low latitudes - which show a linear trend as highlighted by the dotted line. SCR and BSCR are shown as squares, Isidis is represented by a circle, igneous references as diamonds and sedimentary references as triangles. Standard error for average values is displayed in top left as a purple square. Isidis, BSCR and SCR are grouped together at the higher end of observed K and Th abundances. SCR differs from Isidis in overall dispersion of K and Th abundances, with SCR having a much smaller dispersion in values. **(B)** Mean S and Cl values (formatting the same as in 2A), from chemical maps, along with the underlying data used to calculate the mean for reference regions on Mars, as well as S and Cl throughout the low to mid latitudes. MFF and Apollinaris Mons have the highest abundances of S and Cl, with SCR and BSCR reporting the second and third highest values, respectively. The remaining regions all have abundances lower than the crustal average. BSCR has a large dispersion in Cl values, much larger than what is observed for Apollinaris and SCR, both of which vary similarly. BSCR exhibits the largest range in values, whereas Apollinaris, Hellas, and SCR all show comparatively smaller range in S abundance. The remaining regions all exhibit abundances of S and Cl that are lower than the global average, and tend to cluster near each other, independent of provenance.

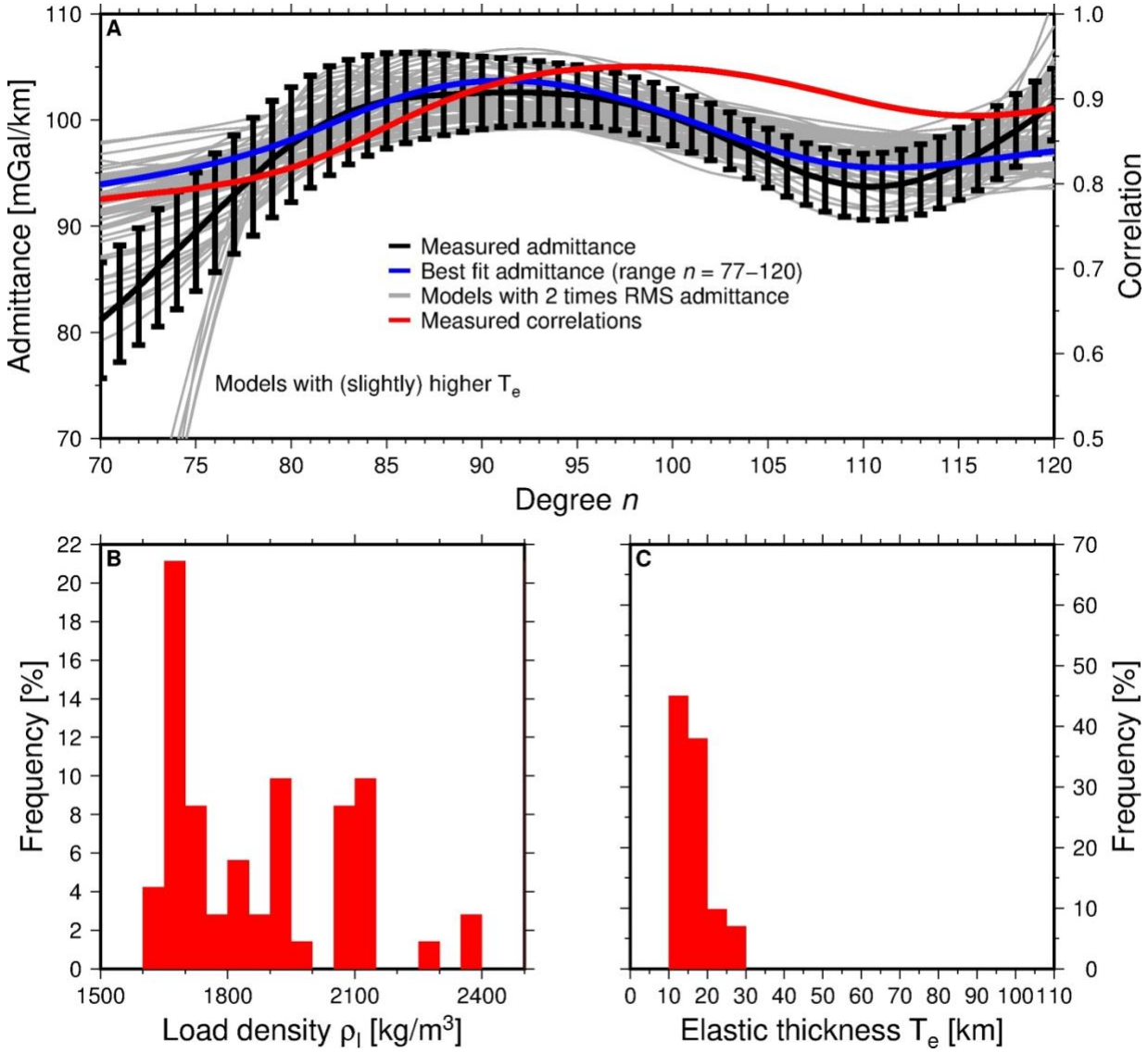

548 **Fig. 3**: Localized admittance and correlation between gravity and topography for the Arabia
549 Terra area (centered on -5˚E,25˚N, for a spherical cap with a radius of 15˚), including the best-fit
550 theoretical admittance and models within two times this best fit (**A**). **A** shows the best-fit
551 admittance model of our geophysical analyses, which has a root-mean-square (RMS) of the
552 misfit between the theoretical model and measured admittance of 1.34 mGal/km for our
553 windowed region (SI Appendix, Fig. S3) (degree range 77-120). The error bounds on the
554 admittance shown in Fig. 3A are computed from the relationship between admittance variance
555 and correlation (Wieczorek, 2008). Histograms of the values for load density (**B**) and elastic
556 thickness (**C**) for the models are also included.

557
558

Geophysical Research Letters

Supporting Information for

Supererruptions in Northwestern Arabia Terra reveal an early stage of Mars' mantle evolution

Augustus Bates[1]*, S. Goossens[2], J. M. Lorenzo[1], L. Ojha[3], D. R. Hood[4], S. Karunatillake[1], S. Kobs Nawotniak[5], T. Paladino[5]

[1]Department of Geology and Geophysics, Louisiana State University, Baton Rouge, LA, USA

[2] NASA Goddard Space Flight Center

[3]Rutgers, The State University of New Jersey

[4]Baylor University

[5]Idaho State University

Contents of this file

Introduction

The following descriptions are available for contextual purposes: region selection justification (text S1), numerical age estimates and compositional analyses methodology details (text S2), and the details of the geophysical modeling detailed methodology (text S3). Each of these sections provides additional details on the methods used to generate the data for the figures presented in the main text as well as the corresponding figures in the supplement.

Text S1. Numerical age estimates and compositional analyses methodology

Numerical age estimates

The Northwest region of Arabia Terra represents one of the oldest terrains on Mars, resulting in geologic heterogeneity that could bias geochemical trends if regional investigations disregard geologic units. Therefore, we examine two regions, the volcanic Super-eruption Context Region (SCR) and Broad-SCR, following mapped geology (K.L. Tanaka et al., 2014), regional geochemistry (Taylor et al., 2010), and topography (Carnes et al., 2017). The Broad-SCR region encloses the smaller SCR region, making chemical comparisons between the two useful for characterizing the distinctness of the chemistry found within SCR. Using our prior delineations (Carnes et al., 2017), we calculated a crater-based age for both Arabia regions. We use two complementary methods for the purpose: 1) crater-based numerical average (Fig. S1B), calculated using CratercountsII software (Arvidson et al., 1979; Hartmann et al., 2001; Werner & Tanaka, 2011) and 2) mapped geology based categorical age distribution (Fig. S1A) (K.L. Tanaka et al., 2014). Our crater-based age was derived using the CratercountsII software in conjunction with ArcGIS. We manually map craters by defining the rim of a crater with 3 points, to which a circle was then fit. We then used our manually mapped craters to calculate an age using CraterstatsII, with a diameter cutoff of 16 km, which gives a more precise age fit to the geochrons (Hartmann et al., 2001; Werner & Tanaka, 2011). Both methods allowed us to validate our age analyses over the areas, as crater-based dating methods become increasingly biased as area decreases, while mapped geology primarily yields a categorical relative age (Arvidson et al., 1979).

Compositional analyses

The GRS-derived gamma spectra archived at the PDS are the source of our chemical maps, as also used in prior works (Baratoux et al., 2011; Don R. Hood et al., 2019; Donald R. Hood et al., 2016; Ojha et al., 2019; Parro et al., 2017; Susko et al., 2017). The derivation follows the published spectra-to-chemistry modeling methods (Boynton et al., 2007; Evans et al., 2006; Karunatillake et al., 2007). Due to the nature of the derivation methods (e.g., elements like Fe and Si, with abundances determined from scatter and capture nuclear reactions induced by the galactic cosmic fluxes), the chemical maps are generally restricted to the mid-to-low latitudes where H abundances are sufficiently low. Likewise, GRS data provide the chemistry for nine major elements to decimeter depths below the martian surface, likely deeper than the surface dust cover (Ruff & Christensen, 2002) for the martian midlatitudes. The percentage mass fraction (wt%) of the elements discussed in this study, including Si, Ca, and stoichiometric H_2O, are binned into 5° × 5° pixels primarily across the mid-to-low latitudes (roughly 60° to -60°).

Given the insight from the four elements (chemical and geophysical trends section in the manuscript), we compare K, Th, S and Cl from notable Noachian volcanic regions (i.e., Thaumasia Planum, Hesperia Planum and Apollinaris Mons) as well as Argyre, Hellas, Isidis and Eridania sedimentary regions to assess the inter- and intra-regional chemical

trends in igneous and sedimentary settings. We notably exclude H_2O analyses, due to the difficulties in attributing any H_2O abundance trends to a particular process. That is primarily a result of H_2O's varying phases and chemical affinities through different timescales as well as latitudinal dependence of abundance on the martian surface (Clifford et al., 2010; Feldman et al., 2004). In addition, mineral abundance alone cannot account for all measured H_2O (Fialips et al., 2005), making it difficult to attribute a measured H_2O abundance to a specific process or the prevalence of a given mineral group.

The data for each sedimentary and volcanic region are extracted as pixels from the chemical maps with centroid latitude and longitude that falls within each delineated area. For context on a chemical signature from volcanic eruptions in SCR, we examine S and Cl trends in bivariate space across the aforementioned regions, along with reported mean values of S and Cl from the MFF given its possibly pyroclastic origin (Ojha et al., 2018). We analyze K and Th similarly, particularly relative to the linear global trend between the two elements (Taylor et al., 2006). From that, relative enrichments in K and Th become evident between our selected regions and their degree of divergence from the linear trend provides insight into possible alteration processes. We compare these results with the rest of the GRS dataset, as a proxy for the average composition of the martian crust (Karunatillake et al., 2011). We report errors of the average abundances of K, Th, S and Cl. We estimate K/Th uncertainty as $(K/Th)[(\sigma_K/K)^2+(\sigma_{Th}/Th)^2]^{1/2}$, where K and Th are the mean concentration of K, Th (Taylor et al., 2006). The same method is used for S/Cl, where abundances of K and Th are substituted for S and Cl, respectively. Sigma is the propagated numerical uncertainty associated with the mean values of the elements in question.

The crustal reference in Fig. S2 reveals several key trends. The Si content in SCR is slightly enriched compared to the martian crust, consistent with sourcing from a dry, depleted mantle during the transition from Noachian to Hesperian (Balta & McSween, 2013). Ca shows a much higher degree of enrichment, also consistent with a mantle source during this same transition, as there is a shift to more high-Ca pyroxene content over low-Ca at the Noachian/Hesperian boundary (Baratoux et al., 2013). H_2O enrichment can be attributed to efficient scavenging of water – possibly as nucleated ice -- from the martian atmosphere via pyroclasts (Wilson & Head, 2007), if we discount the temporal instability of water on Mars. Furthermore, density estimates are consistent with ice-rich material (Ojha & Lewis, 2018), where ice may sublimate post-deposition creating fretted terrains, a common feature within Arabia and SCR (Denton & Head, 2019).

Text S2. Region Selection

Based on the derived SCR age, we identify three contemporaneous Noachian volcanic provinces as type references for compositional comparisons: Thaumasia Planum, Hesperia Planum, and Apollinaris Mons. These igneous references were chosen based on age overlap with SCR and areal extent. Sufficient spatial scale is necessary when using GRS data as sampling bias becomes more prominent when area decreases. This is primarily a function of GRS's coarse resolution (450 km/pixel; Hood et al., 2016); it is most useful for investigating regional trends, not at the scale of individual craters or paterae. Our three igneous references also cover a wide range of eruptive styles, as Apollinaris is inferred to have erupted explosively in its past (Kerber & Head, 2010). Hesperia and Thaumasia are large igneous provinces that were active during the Late Noachian and Early Hesperian, which may contain compositional trends of magma across this boundary in time.

We also selected several sedimentary references (Isidis, Hellas, Argyre and Eridania) that have similar ages as SCR. Among the references, we regard Isidis' chemistry to represent igneous processes as its Middle Noachian (Ehlmann et al., 2011) formation includes extensive volcanic resurfacing from impact induced magmatism. This resulted in two distinct olivine-rich layers that are km-scale in thickness (Hamilton et al., 2003; Mustard et al., 2009). While there is substantial geomorphological evidence for abundant fluvial activity around and within Isidis, much of it dissipated post-impact (Mustard et al., 2009). Had fluvial activity persisted after the Isidis olivine-rich layer formed, pervasive alteration would have resulted because olivine alters readily, but there is little evidence for such large scale alteration (Mustard et al., 2009). The olivine layer has also been hypothesized to underlie material within the Isidis basin, and extend laterally outward (Boyce et al., 2006). Since the olivine unit is the dominant underlying bedrock layer, the regolith was likely derived primarily from mechanical erosion of the olivine layer with minimal chemical weathering (Newsom et al., 2007). That scenario would result in an overall igneous chemistry at the scale of our chemical maps. Furthermore, Syrtis Major's eruptions could have deposited fine grained volcaniclastic material within the low topography of Isidis (Kerber et al., 2012), particularly given spatial proximity.

We regard Hellas as a reference for low-pH alteration of mafic chemistry. Hellas is hypothesized to have been formed by an impact somewhat earlier and more energetic than Isidis (Ehlmann et al., 2011), which resulted in magmatism around the basin. This magmatism created volcanic edifices surrounding the basin rim, which deposited volcanic units within the basin itself. Hellas is an area of extremely low topography and surrounding volcanics, all of which have contributed basin sediment (Moore & Edgett, 1993; Salese et al., 2016; Kenneth L. Tanaka, 2002). However, prior work has interpreted chemical data within Hellas as evidence for regional low-pH alteration within the basin (Zalewska, 2013) which is corroborated by the numerous valley networks along Hellas' rim (Grau Galofre et al., 2020). These valley networks were likely contemporaneous with the surrounding volcanics or post-date them, as fluvial activity peaked in the Hesperian (Grau Galofre et al., 2020). Therefore, it is likely that the chemistry of the basin floor is

heavily altered and would best described as aqueous alteration of basalt and sulfate formation through evaporation of water (Zalewska, 2013).

We chose a sedimentary reference to the east of Hellas, which we call Eridania for brevity, comprised of highland geologic units that show evidence of heavy fluvial erosion and feature a variety of depositional processes ranging from eolian and fluvial to ash fall (Mest & Crown, 2014; K.L. Tanaka et al., 2014). Our delineation of this region differs from prior works (Michalski et al., 2017), as we focus on portions of this area that are sedimentary in origin and have been heavily weathered (Mest & Crown, 2014; K.L. Tanaka et al., 2014). Eridania, which contains parts of Promethei Terra and Eridania Planitia, is comprised of 2 generalized units: a Hesperian and Noachian undivided unit and a Noachian highland undivided unit (K.L. Tanaka et al., 2014). The former is described as friable, likely containing sedimentary, volcanic and impact rocks and has been altered by weathering. The latter is more representative of occasional tectonic contraction (K.L. Tanaka et al., 2014). A more descriptive geologic analysis of the western portion of the area suggests deposition under lacustrine settings (Mest & Crown, 2014). Therefore, for this study, Eridania represents a mixture of material from a variety of depositional mechanisms that has been heavily altered by weathering.

For our final sedimentary reference, we selected Argyre as it is another impact-formed depositional basin. Prior works have also shown that it lacks convincing proximal or interior volcanics, implying deposition through secondary processes (Kerber et al., 2012). The Argyre deposits show evidence of heavy erosion, primarily by eolian processes with some modification through glacial activity (Kerber et al., 2012), and are hypothesized to be derived from fluvial and glacial activity throughout its early evolution (Dohm et al., 2015). Therefore, Argyre exemplifies bulk regolith sedimentary fill as thoroughly mixed eolian material weathered in the presence of liquid or frozen water, and secondary influences from volcanism (Dohm et al., 2015; Kerber et al., 2012).

For further insight into S and Cl trends on Mars and within SCR, we also chose the Medusae Fossae Formation (MFF) as a reference. The MFF is one of the largest friable deposits on Mars (Diez et al., 2009; Ojha et al., 2018), and holds the highest observed S and Cl abundances on the martian surface (Ojha et al., 2019). This reference is key to distinguish the provenance of SCR's observed S and Cl abundances, and, in particular, to determine if the observed S and Cl values are consistent with volcanic degassing, similar to what is proposed for the MFF (Diez et al., 2009).

To minimize overlap bias, we exclude SCR and BSCR from the bulk crustal proxy constituted of the entire mid-to-low latitudinal areas. In the ensuing analyses, we examine the geochemical consistency between SCR and the reference region types: volcanic, sedimentary basins, and impact-induced magmatism to investigate the provenance of SCR's chemistry.

Text S3. Geophysical modeling methodology

For our geophysical estimations, we use topographic data from the Mars Orbiter Laser Altimeter (MOLA), archived at NASA PDS, and used in the MarsTopo2600 model (M. A. Wieczorek, 2015). The gravity model used in our analysis is at the NASA Goddard Space Flight Center's Planetary Geodynamics Data Archive. From these data, we analyze the admittance between gravity and topography to determine parameters related to the structure of the crust and the loads on the crust used in the modeling. The admittance can be expressed as the transfer function between topography and gravity and contains important information about the structure and processes in the crust. It is defined as the cross-power of the functions divided by the power of topography (M. A. Wieczorek, 2015). When both are expressed in spherical harmonics of degree n and order m, and the cross-power is defined as $S_{gt}(n) = \sum_{m=-n}^{m=n} g_{nm} t_{nm}$, where g_{nm} and t_{nm} are the spherical harmonics coefficients of gravity g and topography t, respectively, the admittance $Z(n)$ is then expressed as $Z(n) = S_{gt}(n)/S_{tt}(n)$. In addition, correlations per degree n are defined as: $\gamma(n)=Sgt(n)/sqrt(S_{gg}(n)S_{tt}(n))$.

For our geophysical analysis, we used a localized spectral approach (Mark A. Wieczorek & Simons, 2005, 2007) to compute localized admittance and correlations. Our spherical cap has a radius of 15˚ and is centered on -5˚E, 25˚N (Fig. S3, Table S1). We use one taper with a bandwidth of L_{win}=30 such that the concentration of the taper is 99.99%. We use the degree and order 150 expansion of Mars' gravity field, which was specifically derived to maintain high correlations with topography, while the power in the model was still fully determined by the data (Goossens et al., 2017), and the MarsTopo2600 model for topography (M. A. Wieczorek, 2015), which is based on Mars Orbiter Laser Altimeter (MOLA) data (Smith et al., 2001). While in general a multi-taper approach is preferred to reduce the errors in the estimated spectra (Mark A. Wieczorek & Simons, 2005), the current resolution of the models does not allow such an analysis.

To prepare the measured admittance and correlations from the topography and gravity field models, we downward continue the gravity field model to the average radius in the area of interest (~3390 km) and then compute the localized admittance and correlation. We then compute theoretical admittance models and compare them to the measured admittance. For the theoretical models, we use the formulation and model of admittance from a prior work (Grott & Wieczorek, 2012) to conduct our analyses. We use both top (or surface) and bottom (or subsurface) loading in our admittance model, and they are assumed to be in phase, and thus correlations between gravity and topography should be unity. In future work, fitting admittance and correlation separately could be considered. Under the assumption that correlations less than unity are due to unmodeled gravitational signals that are uncorrelated with topography, the variance of the admittance is directly related to the correlation per spherical harmonic degree (M. A. Wieczorek, 2015; Mark A. Wieczorek, 2008). For correlations larger than 0.8, the signal-to-noise is 1.78, and we find correlations > 0.8 for spherical harmonics degrees > 77 for our chosen localization.

We thus use the degree range 77-120 to fit theoretical admittance models that depend on the following parameters: crustal density, load density, crustal thickness, elastic

thickness, load depth, and load ratio. The load ratio L is defined such that it varies between -1 and (see Grott & Wieczorek, 2012), with $L > 0$ corresponding to subsurface and surface loads of the same sign, and $L < 0$ to those of opposite sign. Because we use the degree and order 150 expansion for the gravity field model as presented by Goossens et al. (2017), we can use degree 120 as the upper limit, since the upper limit is determined from L_{max}-L_{win} (Mark A. Wieczorek & Simons, 2005, 2007). Correlations for this model are still sufficiently high as stated above (see also Fig. 4A and S4) and this allows us to increase the degree range over which to fit the theoretical model, compared to using a degree and order 120 expansion which would only allow the range 77-90.

We apply a straightforward grid search to find the best-fit admittance models in the 77-120 degree range, by computing the theoretical admittance for each parameter combination, and applying the same downward continuation and localization as we applied to the measured admittance. The grid bounds for our search are given in Table S1. Using those bounds and step size (Table S1), we evaluate roughly 40 million models. For each model, we compute the root-mean-square (RMS) of the difference between theoretical and measured admittance over the degree range 77-120.

Next, from the 40 million models, we select only those that fit the admittance within twice the best-fit RMS (which is the lowest RMS we find in the entire set). That results in a sub-selection of eventually only 71 models. We investigate the spread in the parameter values from the sub-selection to establish which parameters can be constrained, keeping in mind that while our search space was large, the sub-selection is only a tiny part of this. A more directed search or finer step-sizes around the best-fit parameters would increase the number but we do not expect that the overall picture would change much.

We find that the best-constrained parameters are the load density and elastic thickness. We define "best-constrained" as those parameters from the best-fit collection for which the histograms of their spread show some concentration around certain values, as opposed to parameters that show a flat histogram that spans their entire range. Based on the spread in the estimated values, load density and elastic thickness show the most reasonably clustered histograms. Other parameters were estimated, but ensuing histograms were inconclusive in terms of an overall trend towards either low or high values. The load ratio is also reasonably constrained, and we specifically find that the inclusion of bottom loading improves the fit greatly: a top-loading model without bottom loading cannot map the admittance signal and results in a much higher RMS of fit. We did model this region with a top-only loading model, but it failed to capture the entirety of the admittance signal. Thus, we employed a mixed loading model which was better suited to capturing the entire admittance signal. The crustal density, crustal thickness and load depth show a large spread and cannot be determined robustly. This work thus considers only these two parameters in its discussion of SCR's provenance. In summary, only models with mixed bottom and top loading, low elastic thickness and a load density of ~1500 kg/m^3 were suitable to account for the observed admittance signal. This motivates future work which considers simultaneous fitting of admittance and correlation, using loads that are out of phase, for additional insight into the unusual crust-mantle boundary conditions within NW Arabia during Noachian Mars.

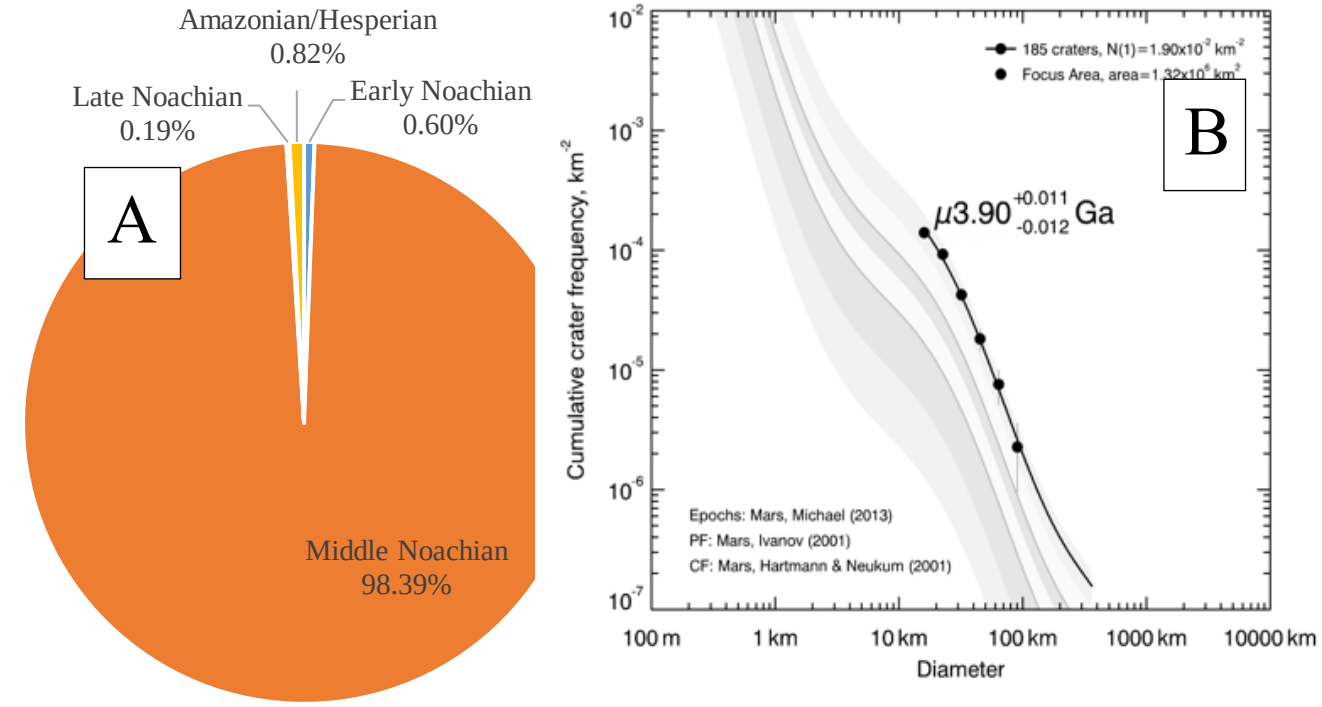

Figure S1, (A): Pie chart showing the areal distribution of geologic age categories for SCR, using mapped geology (CITATION FORMAT! 1). The predominant geologic age is Middle Noachian which constitutes ~98% of the area in SCR. The remaining ~2% of terrain mostly corresponds to younger eon(s). The chart primarily describes the landscape age distribution, so it effectively characterizes the age of material analyzed through chemical maps. **(B)**: Crater-counting derived average numeric age for SCR. The calculated age from crater counting corresponds to the Middle Noachian (3.8 -3.9 Ga), which agrees with mapped-geology of (A). The spectrum of gray bands (Fig S1, B) is the martian chronostratigraphic age divisions, which are used to determine numerical age from crater data.

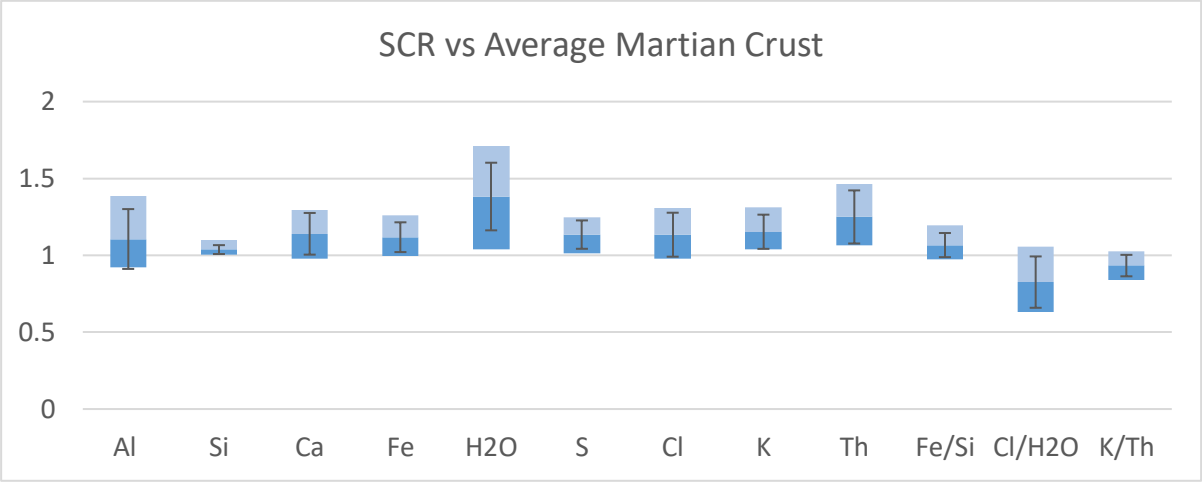

Figure S2: All elements measured by GRS within SCR compared to the average martian crust. The average crust is all the data from the GRS instrument, with SCR removed, thus providing a comparison between SCR and the rest of the dataset. This plot shows SCR compared to the Martian crust. Boxes are bound by ratio of $75^{th}/25^{th}$ %-ile, $50^{th}/50^{th}$, $25^{th}/75^{th}$ to visually summarize the distributional comparison for any given element between two areas. Where the $50^{th}/50^{th}$ %-ile lies on y=1, the median value of that element is the same between both regions. Error bars are propagated ratios of the median absolute deviations, capturing the deviation of values from the corresponding medians. SCR is enriched in every analyzed element compared to the crust, with notable enrichments in Si, Ca and H_2O.

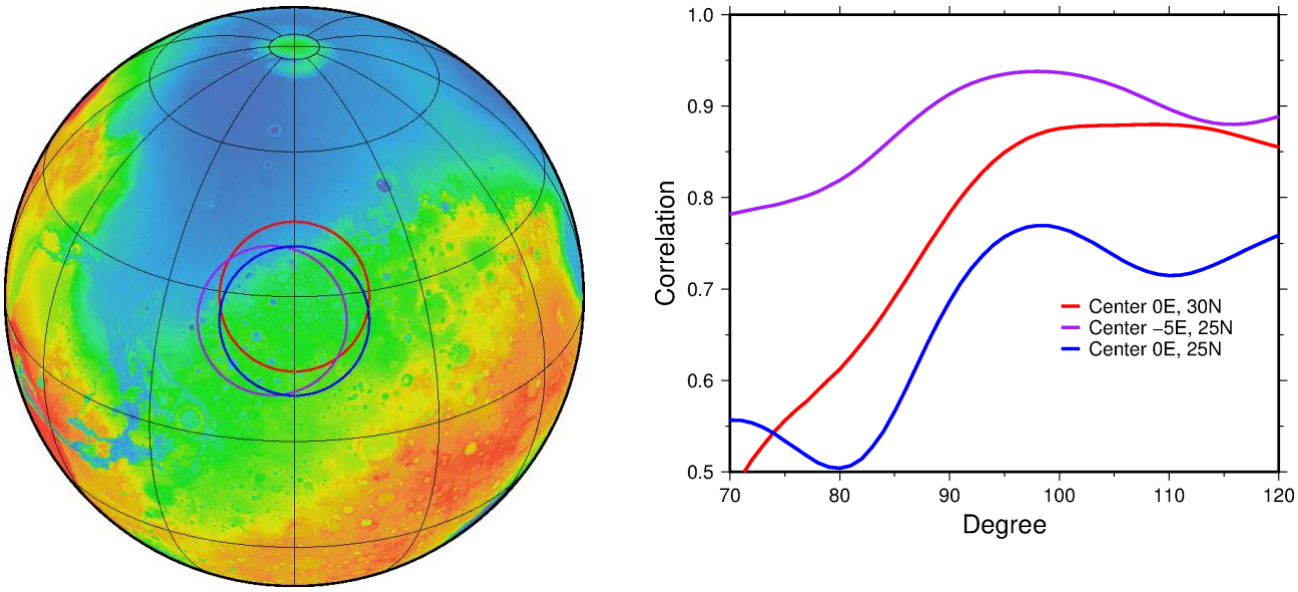

Figure S3: We considered several different localization windows, both in a search for a sufficient correlation between topography and gravity and a radius that accurately encompassed SCR. The purple circle reflects the most geographically accurate outline for SCR, and also shows the highest correlation (> 0.8) across the window. Other windows (red, blue) showed sufficient correlations, suggesting that our final window selection is not an outlier in comparison to other windows within Arabia. The purple localization was then used to estimate geophysical parameters, which are summarized in Table S2. High correlations between gravity and topography are preferred: results follow for center at -5˚E, 25˚N (purple), but there are relatively high correlations for regions in the immediate vicinity of the SCR.

Table S1: A list of the parameters that are varied in our grid search for a best fit theoretical admittance model, including the range applied and the step size taken.

Parameter [unit]	Range	Step size
Crustal thickness [km]	5-100	5
Elastic thickness [km]	5-150	5
Crustal density [kg/m^3]	2400-3100	50
Load density [kg/m^3]	1600-2500	50
Load depth [km]	5 - 100	10
Load ratio [no unit]	-0.95-0.95	0.1
Note: load depth cannot exceed crustal thickness		

References

Arvidson, R. E., Boyce, J., Chapman, C., Cintala, M., Fulchignoni, M., Moore, H., et al. (1979). Standard Techniques for Presentation and Analysis of Crater Size-Frequency Data. *Icarus*, *474*, 467–474. https://doi.org/10.1016/0019-1035(79)90009-5

Balta, J. B., & McSween, H. Y. (2013). Water and the composition of Martian magmas. *Geology*, *41*(July), 1115–1118. https://doi.org/10.1130/G34714.1

Baratoux, D., Toplis, M. J., Monnereau, M., & Gasnault, O. (2011). Thermal history of Mars inferred from orbital geochemistry of volcanic provinces. *Nature*, *472*(7343), 338–41. https://doi.org/10.1038/nature09903

Baratoux, D., Toplis, M. J., Monnereau, M., & Sautter, V. (2013). The petrological expression of early Mars volcanism. *Journal of Geophysical Research E: Planets*, *118*(1), 59–64. https://doi.org/10.1029/2012JE004234

Boyce, J. M., Mouginis-Mark, P., Garbeil, H., & Tornabene, L. L. (2006). Deep impact craters in the Isidis and southwestern Utopia Planitia regions of Mars: High target material strength as a possible cause. *Geophysical Research Letters*, *33*(6), 2–5. https://doi.org/10.1029/2005GL024462

Boynton, W. V., Taylor, G. J., Evans, L. G., Reedy, R. C., Starr, R., Janes, D. M., et al. (2007). Concentration of H, Si, Cl, K, Fe, and Th in the low- and mid-latitude regions of Mars. *Journal of Geophysical Research*, *112*, E12S99. https://doi.org/10.1029/2007JE002887

Carnes, L. L., Karunatillake, S., Susko, D. A., & Hood, D. R. (2017). Delineating the Arabia Terra region on Mars to investigate paterae orgins. In *LPSC2017* (p. Abstract 1756). https://doi.org/10.1038/ngeo2845

Clifford, S. M., Lasue, J., Heggy, E., Boisson, J., McGovern, P., & Max, M. D. (2010). Depth of the Martian cryosphere: Revised estimates and implications for the existence and detection of subpermafrost groundwater. *Journal of Geophysical Research*, *115*(E7), 1–17. https://doi.org/10.1029/2009je003462

Denton, A., & Head, J. W. (2019). FRETTED CHANNELS AND CLOSED DEPRESSIONS IN NORTHERN ARABIA TERRA, MARS: ORIGINS AND IMPLICATIONS FOR SUBSURFACE HYDROLOGIC ACTIVITY. *LPSC 2019 Abstract*, (1082), 10–11.

Diez, B., Feldman, W. C., Mangold, N., Baratoux, D., Maurice, S., Gasnault, O., et al. (2009). Contribution of Mars Odyssey GRS at Central Elysium Planitia. *Icarus*, *200*(1), 19–29. https://doi.org/10.1016/j.icarus.2008.11.011

Dohm, J. M., Hare, T. M., Robbins, S. J., Williams, J. P., Soare, R. J., El-Maarry, M. R., et al. (2015). Geological and hydrological histories of the Argyre province, Mars. *Icarus*, *253*, 66–98. https://doi.org/10.1016/j.icarus.2015.02.017

Ehlmann, B. L., Mustard, J. F., Murchie, S. L., Bibring, J.-P., Meunier, A., Fraeman, A. a., & Langevin, Y. (2011). Subsurface water and clay mineral formation during the early history of Mars. *Nature*, *479*(7371), 53–60. https://doi.org/10.1038/nature10582

Evans, L. G., Reedy, R. C., Starr, R. D., Kerry, K. E., & Boynton, W. V. (2006). Analysis of gamma ray spectra measured by Mars Odyssey. *Journal of Geophysical Research*, *112*(E3), E03S04. https://doi.org/10.1029/2005JE002657

Feldman, W. C., Prettyman, T. H., Maurice, S., Plaut, J. J., Blish, D. L., Vaniman, D. T.,

et al. (2004). Global distribution of near-surface hydrogen on Mars. *Journal of Geophysical Research*, *109*(E9), E09006. https://doi.org/10.1029/2003JE002160

Fialips, C. I., Carey, J. W., Vaniman, D. T., Bish, D. L., Feldman, W. C., & Mellon, M. T. (2005). Hydration state of zeolites, clays, and hydrated salts under present-day martian surface conditions: Can hydrous minerals account for Mars Odyssey observations of near-equatorial water-equivalent hydrogen? *Icarus*, *178*(1), 74–83. https://doi.org/10.1016/j.icarus.2005.04.020

Goossens, S., Mazarico, E., Sabaka, T. J., Nicholas, J. B., Genova, A., & Neumann, G. A. (2017). Evidence for a low bulk crustal density for Mars from gravity and topography. *Geophysical Research Letters*, *44*(15), 7686–7694. https://doi.org/10.1002/2017gl074172

Grau Galofre, A., Bahia, R. S., Jellinek, A. M., Whipple, K. X., & Gallo, R. (2020). Did Martian valley networks substantially modify the landscape? *Earth and Planetary Science Letters*, *547*, 116482. https://doi.org/10.1016/j.epsl.2020.116482

Grott, M., & Wieczorek, M. A. (2012). Density and lithospheric structure at Tyrrhena Patera, Mars, from gravity and topography data. *Icarus*, *221*(1), 43–52. https://doi.org/10.1016/j.icarus.2012.07.008

Hamilton, V. E., Christensen, P. R., McSween, H. Y., & Bandfield, J. L. (2003). Searching for the source regions of martian meteorites using MGS TES: Integrating martian meteorites into the global distribution of igneous materials on Mars. *Meteoritics and Planetary Science*, *38*(6), 871–885. https://doi.org/10.1111/j.1945-5100.2003.tb00284.x

Hartmann, W. K., Neukum, G., Zentrum, D., & Berlin, D.-. (2001). CRATERING CHRONOLOGY AND THE EVOLUTION OF MARS 1 . Background : Cratering Studies and the Relation to Martian Rocks Through the process of impact cratering , Nature randomly stamps circular bowls of known shape on planetary surfaces . This fact offers us . *Nature*, (February), 165–194.

Hood, Don R., Karunatillake, S., Gasnault, O., Williams, A. J., Dutrow, B. L., Ojha, L., et al. (2019). Contrasting Regional Soil Alteration across the Topographic Dichotomy of Mars. *Geophysical Research Letters*, 1–10. https://doi.org/10.1029/2019GL084483

Hood, Donald R., Judice, T., Karunatillake, S., Rogers, D., Dohm, J. M., Susko, D. A., & Carnes, L. K. (2016). Assessing the geologic evolution of Greater Thaumasia, Mars. *Journal of Geophysical Research: Planets*, *121*(9), 1753–1769. https://doi.org/10.1002/2016JE005046

Karunatillake, S., Keller, J. M., Squyres, S. W., Boynton, W. V, Janes, D. M., Gasnault, O., & Newsom, H. E. (2007). Chemical compositions at Mars landing sites subject to Mars Odyssey Gamma Ray Spectrometer constraints. *Journal of Geophysical Research*, *112*, 1–16. https://doi.org/10.1029/2006JE002859

Karunatillake, S., Squyres, S. W., Gasnault, O., Keller, J. M., Janes, D. M., Boynton, W. V., & Finch, M. J. (2011). Recipes for Spatial Statistics with Global Datasets: A Martian Case Study. *Journal of Scientific Computing*, *46*(3), 439–451. https://doi.org/10.1007/s10915-010-9412-z

Kerber, L., & Head, J. W. (2010). The age of the Medusae Fossae Formation: Evidence of Hesperian emplacement from crater morphology, stratigraphy, and ancient lava contacts. *Icarus*, *206*(2), 669–684. https://doi.org/10.1016/j.icarus.2009.10.001

Kerber, L., Head, J. W., Madeleine, J.-B., Forget, F., & Wilson, L. (2012). The dispersal of pyroclasts from ancient explosive volcanoes on Mars: Implications for the friable layered deposits. *Icarus*, *219*(1), 358–381. https://doi.org/10.1016/j.icarus.2012.03.016

Mest, S., & Crown, D. (2014). Scientific Investigations Map 3245 Geologic Map of MTM – 30247 , – 35247 and – 40247 Quadrangles, Reull Vallis Region of Mars. *USGS Publication*. Retrieved from https://pubs.usgs.gov/sim/3245/pdf/sim3245_pamphlet.pdf

Michalski, J. R., Dobrea, E. Z. N., Niles, P. B., & Cuadros, J. (2017). Ancient hydrothermal seafloor deposits in Eridania basin on Mars. *Nature Communications*, *8*(May), 15978. https://doi.org/10.1038/ncomms15978

Moore, J. M., & Edgett, K. S. (1993). Hellas Planitia, Mars: Site of Net Dust Erosion and Implications for the Nature of Basin Floor Deposits, *20*(15), 1599–1602.

Mustard, J. F., Ehlmann, B. L., Murchie, S. L., Poulet, F., Mangold, N., Head, J. W., et al. (2009). Composition, morphology, and stratigraphy of Noachian crust around the Isidis basin. *Journal of Geophysical Research E: Planets*, *114*(12), 1–18. https://doi.org/10.1029/2009JE003349

Newsom, H. E., Crumpler, L. S., Reedy, R. C., Petersen, M. T., Newsom, G. C., Evans, L. G., et al. (2007). Geochemistry of Martian soil and bedrock in mantled and less mantled terrains with gamma ray data from Mars Odyssey. *Journal of Geophysical Research*, *112*, E03S12. https://doi.org/10.1029/2006JE002680

Ojha, L., & Lewis, K. (2018). The Density of the Medusae Fossae Formation: Implications for its Composition, Origin, and Importance in Martian History. *Journal of Geophysical Research: Planets*, *123*(6), 1368–1379. https://doi.org/10.1029/2018JE005565

Ojha, L., Lewis, K., Karunatillake, S., & Schmidt, M. (2018). The Medusae Fossae Formation as the single largest source of dust on Mars. *Nature Communications*, *9*(1), 1–7. https://doi.org/10.1038/s41467-018-05291-5

Ojha, L., Karunatillake, S., & Lacovino, K. (2019). Atmospheric Injection of Sulfur from the Medusae Fossae Forming Events. *Planetary and Space Science*, *179*, 104734. https://doi.org/10.1016/j.pss.2019.104734

Parro, L. M., Jiménez-Díaz, A., Mansilla, F., & Ruiz, J. (2017). Present-day heat flow model of Mars. *Scientific Reports*, *7*(April 2017), 45629. https://doi.org/10.1038/srep45629

Ruff, S. W., & Christensen, P. R. (2002). Bright and dark regions on Mars: Particle size and mineralogical characteristics based on Thermal Emission Spectrometer data. *Journal of Geophysical Research*, *107*(E12), 5127. https://doi.org/10.1029/2001JE001580

Salese, F., Ansan, V., Mangold, N., Carter, J., Ody, A., Poulet, F., & Ori, G. G. (2016). A sedimentary origin for intercrater plains north of the Hellas basin: Implications for climate conditions and erosion rates on early Mars. *Journal of Geophysical Research: Planets*, *121*(11), 2239–2267. https://doi.org/10.1002/2016JE005039

Smith, D. E., Head, J. W., Muhleman, D. O., Pettengill, G. H., Phillips, R. J., Solomon, S. C., et al. (2001). Mars orbiter laser altimeter: Experiment summary after the first year of global mapping of Mars. *Journal of Geophysical Research E: Planets*, *106*(10), 23689–23722.

Susko, D. A., Karunatillake, S., Kodikara, G., Skok, J. R., Wray, J., Heldmann, J., et al. (2017). A record of igneous evolution in Elysium, a major martian volcanic province. *Scientific Reports*, *7*, 43177. https://doi.org/10.1038/srep43177

Tanaka, K.L., Robbins, S. J., Fortezzo, C. M., Skinner, J. A., & Hare, T. M. (2014). The digital global geologic map of Mars: Chronostratigraphic ages, topographic and crater morphologic characteristics, and updated resurfacing history. *Planetary and Space Science*, *95*, 11–24. https://doi.org/10.1016/j.pss.2013.03.006

Tanaka, Kenneth L. (2002). Catastrophic erosion of Hellas basin rim on Mars induced by magmatic intrusion into volatile-rich rocks. *Geophysical Research Letters*, *29*(8), 1–4. https://doi.org/10.1029/2001GL013885

Taylor, G. J., Stopar, J. D., Boynton, W. V., Karunatillake, S., Keller, J. M., Brückner, J., et al. (2006). Variations in K/Th on Mars. *Journal of Geophysical Research*, *112*(E3), E03S06. https://doi.org/10.1029/2006JE002676

Taylor, G. J., Martel, L. M. V., Karunatillake, S., Gasnault, O., & Boynton, W. V. (2010). Mapping Mars geochemically. *Geology*, *38*(2), 183–186. https://doi.org/10.1130/G30470.1

Werner, S. C., & Tanaka, K. L. (2011). Redefinition of the crater-density and absolute-age boundaries for the chronostratigraphic system of Mars. *Icarus*, *215*(2), 603–607. https://doi.org/10.1016/j.icarus.2011.07.024

Wieczorek, M. A. (2015). *Gravity and Topography of the Terrestrial Planets*. *Treatise on Geophysics: Second Edition* (Vol. 10). Elsevier B.V. https://doi.org/10.1016/B978-0-444-53802-4.00169-X

Wieczorek, Mark A. (2008). Constraints on the composition of the martian south polar cap from gravity and topography. *Icarus*, *196*(2), 506–517. https://doi.org/10.1016/j.icarus.2007.10.026

Wieczorek, Mark A., & Simons, F. J. (2005). Localized spectral analysis on the sphere. *Geophysical Journal International*, *162*(3), 655–675. https://doi.org/10.1111/j.1365-246X.2005.02687.x

Wieczorek, Mark A., & Simons, F. J. (2007). Minimum-variance multitaper spectral estimation on the sphere. *Journal of Fourier Analysis and Applications*, *13*(6), 665–692. https://doi.org/10.1007/s00041-006-6904-1

Wilson, L., & Head, J. W. (2007). Explosive volcanic eruptions on Mars: Tephra and accretionary lapilli formation, dispersal and recognition in the geologic record. *Journal of Volcanology and Geothermal Research*, *163*(1–4), 83–97. https://doi.org/10.1016/j.jvolgeores.2007.03.007

Zalewska, N. (2013). Hellas Planitia as a potential site of sedimentary minerals. *Planetary and Space Science*, *78*, 25–32. https://doi.org/10.1016/j.pss.2012.12.006